J Biochem Technol (2024) 15(4): 26-34
https://doi.org/10.51847/Qe4kzCk2DJ
ISSN: 0974-2328

In Silico Investigation of Andrographolide and Resveratrol with DNA-Sensing Inflammasomes AIM2 and IFI16 in Periodontitis

Lalitha Tanjore Arunachalam*, Snophia Suresh, Vamsi Lavu, Shankarram Vedamanickam

Received: 01September 2024 / Received in revised form: 20 November 2024, Accepted: 24 November 2024, Published online: 19 December 2024

Abstract

Proinflammatory cytokines play a critical role in the destruction of periodontal tissues. DNA-sensing inflammasomes, such as AIM2 and IFI16, are key mediators in the secretion of IL-1 and IL-18 and facilitate pyroptosis in periodontitis. Andrographolide and resveratrol are phytocompounds known for their anti-inflammatory effects, though their precise mechanisms of action remain uncertain. This study aimed to elucidate the molecular interactions of andrographolide and resveratrol with AIM2 and IFI16 inflammasomes using a computational approach. Ten phytocompounds were selected and analyzed via molecular docking. Protein-ligand docking was conducted with AutoDock 4.2.6. Binding affinities and hydrogen bond interactions were assessed. Andrographolide and resveratrol complexes with AIM2 and IFI16 were further subjected to 100 ns molecular dynamics simulations using GROMACS software to assess complex stability. Both andrographolide and resveratrol complexes demonstrated stability throughout the simulations, with adequate inter-hydrogen bonding. Molecular Mechanics Poisson-Boltzmann Surface Area (MMPBSA) analysis revealed that AIM2-andrographolide (-112.100 ± 18.106 kJ/mol) and IFI16-andrographolide (-50.047 ± 27.076 kJ/mol) complexes exhibited higher binding energies compared to AIM2-resveratrol (-15.328 ± 2.539 kJ/mol) and IFI16-resveratrol (-12.534 ± 20.184 kJ/mol) complexes. The results indicate that andrographolide demonstrates a stronger binding affinity to AIM2 and IFI16 inflammasomes compared to resveratrol. This suggests andrographolide is a promising host modulatory candidate for the therapeutic management of periodontitis.

Keywords: Periodontitis, AIM2 inflammasome, IFI16 inflammasome, Andrographolide, Resveratrol, Molecular docking

Lalitha Tanjore Arunachalam*, Snophia Suresh, Shankarram Vedamanickam
Department of Periodontics, Thai Moogambigai Dental College & Hospital, Dr.M.G.R. Educational and Research Institute, Golden George Nagar, Mogappair, Chennai, Tamil Nadu, India 600107.

Vamsi Lavu
Department of Periodontics, Sri Ramachandra Dental College & Hospital, SRIHER University, Ramachandra Nagar, Porur, Chennai, India.

***E-mail:** doclalita@gmail.com

Introduction

Periodontitis is a complex, multifactorial inflammatory condition primarily initiated by the accumulation of pathogenic bacterial biofilms, particularly in susceptible individuals. The progression of periodontitis results in the breakdown of supporting structures of the teeth, including the gingiva, periodontal ligament, and alveolar bone. While periodontal pathogens are known initiators of periodontal pathology, the host's immune response largely dictates the extent of tissue destruction. In response to microbial invasion, host immune cells release an array of pro-inflammatory cytokines, matrix metalloproteinases (MMPs), and reactive oxygen species (ROS) that contribute to the inflammatory microenvironment and exacerbate tissue damage. This dynamic interaction between pathogens and host immune responses is central to the pathogenesis of periodontitis (Cekici *et al*., 2014).

Recent research underscores the role of innate immune sensors known as pattern recognition receptors (PRRs) in recognizing conserved microbial structures, known as pathogen-associated molecular patterns (PAMPs), and endogenous signals released from damaged tissues, called damage-associated molecular patterns (DAMPs). These PRRs, including toll-like receptors (TLRs) and nucleotide-binding oligomerization domain (NOD)-like receptors, are critical in sensing bacterial components and initiating downstream immune responses. Upon activation, these PRRs initiate a cascade that leads to the assembly of inflammasomes—intracellular multiprotein complexes that play a pivotal role in the maturation and secretion of key pro-inflammatory cytokines, particularly interleukin (IL)-1β and IL-18 (Lamkanfi & Dixit, 2014).

Among the various inflammasomes, the absent in melanoma 2 (AIM2) and interferon-inducible protein 16 (IFI16) inflammasomes have gained considerable attention in periodontal research. AIM2 and IFI16 are cytoplasmic sensors that specifically recognize double-stranded DNA (dsDNA), which can be released from both pathogens and damaged host cells. AIM2, upon detecting dsDNA, triggers the recruitment of adapter protein ASC, leading to the activation of caspase-1 and subsequent cleavage and release of mature IL-1β and IL-18. These cytokines not only propagate inflammation but also contribute to cell death via pyroptosis, an inflammatory form of programmed cell death that further promotes tissue destruction (Man *et al*., 2016). IFI16, which belongs to the pyrin family, is unique in that it is localized

both in the nucleus and cytoplasm, allowing it to act as a broader sentinel in immune surveillance (Almine *et al*., 2017).

Studies have shown that pathogenic bacteria in periodontitis, particularly *P. gingivalis*, can activate AIM2 and IFI16 inflammasomes. This activation amplifies the inflammatory cascade, as IL-1β and IL-18 release contribute to enhanced osteoclastogenesis, increased matrix degradation, and persistent inflammation, which are hallmarks of progressive periodontitis. Furthermore, elevated levels of AIM2 and IFI16 inflammasomes in periodontal tissues have been correlated with disease severity, suggesting that these inflammasomes may serve as biomarkers for periodontal disease activity and progression (Marchesan, 2020).

Given the substantial role of inflammasomes in periodontal tissue destruction, recent research has focused on therapeutic strategies to inhibit inflammasome activation. Host-modulatory therapies that target AIM2 and IFI16 represent a promising approach to control excessive inflammation in periodontitis without directly targeting bacterial pathogens, thus avoiding potential issues with antibiotic resistance. In this context, natural phytocompounds have attracted significant interest due to their anti-inflammatory and antioxidant properties, as well as their relatively low toxicity (Papathanasiou *et al*., 2023). Studies exploring the inhibitory effects of phytochemicals on inflammasome activation have demonstrated promising results, showing these compounds' potential to downregulate inflammasome signaling pathways, in various inflammatory conditions (Olcum *et al*., 2020). This study aims to explore the docking interactions of specific phytocompounds with AIM2 and IFI16 inflammasomes using in silico analysis.

Materials and Methods

Protein Preparation

The three-dimensional X-ray crystallographic structure AIM2 (PDB id: 3RN2) and IFI16 (8X70) with the correct resolution were obtained from the Protein data bank database (PDB: http:// www. rcsb. org/ pdb). After retrieval, the structure was pre-processed and refined using AutoDock 4.2.6. It involved the removal of the water molecules from the cavity, the addition of hydrogen atoms, stabilizing the charges using Kollman united atoms, and was saved as a pdbqt file till further analysis.

Selection of Phytocompounds

A comprehensive review by Özenver and Efferth (2021) highlighted various phytochemicals from diverse classes of natural compounds and herbal plants that are effective against the NLRP3 inflammasome. Using this review as a standard reference, we selected ten phytochemicals for further study. The selected compounds, along with their natural sources, compound groups, and modes of action, are summarized in **Table 1**.

Table 1. Characteristics of the selected phytocompounds

Phytocompound	Class	Origin	Actions
Curcumin	Phenolic compound	Rhizomes of turmeric	Antioxidant, anti-inflammatory, insulin-sensitizing, antimicrobial
Girinimbine	Carbazole alkaloid	Curry leaves	antibacterial, anti-inflammatory, and antioxidant
Andrographolide	Terpenoid	Andrographis paniculata, a medicinal herbal plant /Nilavembu	Antiinflammatory
Berberine	Alkaloid	Medicinal herb	antibacterial, antiinflammatory, and antioxidant
Sulforaphane	Organosulfur Compound	Cruciferous vegetables such as broccoli, brussels sprouts, and cabbage	Antiinflammatory
Resveratrol	Phenolic compound	Pines and grapevines	Neuroprotective & anti-inflammatory
Epigallocatechin gallate	Cathechin	Green tea	Antioxidant, antiinflammatory
Mangiferin	Phenolic compound	Mango trees	Antioxidant, antiinflammatory and Antiapoptotic
Oridonin	Diterpenoid	Medicinal herb	Antimicrobial, anti-inflammatory, and neuroregulatory properties
Obovatol	Lignans	Magnolia obovate	Antibacterial, antiplatelet, neuroprotective, antioxidant and anti-inflammatory

Ligand Preparation

The three-dimensional structure of the selected compounds was retrieved from the PubChem database (https://pubchem.ncbi.nlm.nih.gov/) in the structure-data file (SDF) format. The SDF format of the ligand was converted to PDB using OpenBabel Software (https://sourceforge.net/projects/openbabel/). Next, the processing was carried out by adding Gasteiger charges, and the ligand was saved as a pdbqt file.

In Silico Evaluation of Pharmacokinetic, Physicochemical Attributes and Toxicity

Pharmaceutically significant descriptors and physically relevant properties of the ligands were predicted. The physicochemical properties such as molecular weight, molar refractivity, topological polar surface area, number of hydrogen bond donors/number of hydrogen bond acceptors, number of rotatable bonds, and lipophilicity (logP) based on Lipinski's rule of five were carried out with web-based tool - SWISSADME (http:// www. swiss adme.ch/) (Daina *et al*., 2017). It is a user-friendly interface with advanced computational algorithms and aids in evaluating the potential efficacy and safety of the selected compounds. Additionally, the safety profile of the selected phytochemicals was predicted using the web-based computational tool - pkCSM-pharmacokinetics (http:// biosig. unimelb. edu. au/ pkcsm/ prediction). Mangiferin and Epigallocatechin gallate did not comply with the Lipinski rule and hence were not considered for docking analysis.

Molecular Interaction

Docking between the protein and ligand was performed using Auto Dock 4.2.6 (https://autodock.scripps.edu/resource/tools) software. The pdbqt format of ligand and protein was used further for docking. A grid box covering the entire protein structure was constructed and the output was saved as a gpf file. Docking was performed using Lamarckism genetic algorithm and the output was obtained in dlg file format. The molecule with the lowest binding energy obtained was selected to visualize the ligand-protein interaction. The binding affinity and the energy of the selected phytocompounds with AIM2 & IFI16 were compared with that of two selective pharmacological inhibitors, namely niclosamide and 4 sulfonic calixarene.

Molecular Visualisation

Biovia Discovery Studio Visualizer 16.1.0 was used to visualize the molecular interactions (Morris *et al*., 2009). It is a comprehensive molecular modeling and simulation software that offers robust tools for visualizing, analyzing, and modeling molecular structures, interactions, and properties with high precision.

Molecular Dynamics Simulation

An appropriate technique for investigating the structural dynamics of proteins and their interactions with ligands is the application of all-atom MD simulation. It enables a thorough examination of molecular systems at the atomic level, and this method has completely transformed the field of computer-aided drug design and discovery. In this study, MD simulations were carried out to examine the dynamic changes that occur upon binding of the receptor-ligand complex. Several parameters such as RMSD, RMSF, Rg, SASA, and inter-hydrogen bonding was calculated for both the protein and protein-ligand complex.

The selected top ligands were identified from docking analysis such as 3RN2-AND (Andrographolide) and 3RN2-RES (Resveratrol) for AIM2, 8X70-AND (Andrographolide) and 8X70-RES (Resveratrol) for IFI16. The ATB server's ligand topology was chosen. The hydrogens were added to the heavy atoms using the pdb2gmx, a GROMACS module. Using the steepest descent approach, prepared systems were the first to be vacuum minimised by over 1500 steps. The structures were then solvated using a water simple point charge (SPCE) water model in a cubic periodic box. The complex systems were subsequently maintained with an appropriate salt concentration of 0.15 M by adding suitable numbers of Na and Cl counter ions. The system preparation was referred based on a previously published paper (Gangadharappa *et al*., 2020). Each structure that emerged from the NPT equilibration phase underwent a final production run in the NPT ensemble for 100 ns of simulation time. Lastly, the Gromacs software package's many tools—such as the protein root mean square deviation (RMSD), root mean square fluctuation (RMSF), radius of gyration (RG), solvent accessible surface area (SASA), and hydrogen bonding (H-Bond)—were used to analyse the simulation's trajectory. The molecular Mechanics Poisson-Boltzmann surface area (MM-PBSA) approach was employed to understand the binding free energy (3RN2-AND, 3RN2-RES, 8X70-AND and 8X70-RES binding) of an inhibitor with protein over simulation time. A GROMACS utility g_mmpbsa was employed to estimate the binding free energy (Kumari *et al*., 2014). To obtain an accurate result, the four complexes were computed for the last 50 ns with dt 1000 frames.

Results and Discussion

Of the ten phytocompounds, mangiferin and epigallocatechin gallate did not satisfy Lipinski's rule of five and hence were not taken for docking analysis. The other 8 compounds and the selective inhibitors, niclosamide and 4 sulfonic calixarene were considered for further analysis.

The binding affinity, interacting amino acids, bond types, and bond lengths of the selected ligands with AIM2 are detailed in **Table 2**. The binding energies of these ligands to AIM2 were as follows: -6.80 kcal/mol (Curcumin), -6.54 kcal/mol (Girinimbine), -7.26 kcal/mol (Andrographolide), -7.03 kcal/mol (Berberine), -4.16 kcal/mol (Sulforaphane), -6.54 kcal/mol (Resveratrol), -7.39 kcal/mol (Oridonin), -7.26 kcal/mol (Obovatol), -8.85 kcal/mol (Niclosamide), and -10.54 kcal/mol (4-sulfonic calixarene) **(Figure 1)**. These results indicate that 4-sulfonic calixarene, as a pharmacologic inhibitor, exhibited the highest binding affinity to AIM2, followed by Niclosamide. Among the phytocompounds, Oridonin demonstrated the strongest affinity, followed by Andrographolide, Obovatol, Berberine, and Curcumin, while Sulforaphane showed the lowest affinity.

In terms of hydrogen bonding, 4-sulfonic calixarene formed six hydrogen bonds with AIM2. Andrographolide showed the highest number of hydrogen bonds among the phytocompounds, with four bonds to AIM2. This was followed by Resveratrol, Obovatol, and Niclosamide, each forming three hydrogen bonds, while Curcumin, Girinimbine, Berberine, and Oridonin each formed two hydrogen bonds.

Table 2. Docking analysis of AIM2 with selected phytocompounds

Ligand	No of hydrogen bonds	Interacting amino acid	Interacting bonds	Bond length
Curcumin	2	*Thr249, Asn265, Val264, Gly217, Lys245, Glu248*	Conventional hydrogen bond, Carbon-hydrogen bond, Pi-Anion, Pi-Alkyl	Hydrogen bond (Lys 245= 2.17, Asn265= 2.14), Carbon-hydrogen bond (*Thr249*= 2.84, Val264= 3.38, Gly217 =2.87) Pi anion (Glu 248= 3.66), Pi-alkyl (Lys245= 4.27)
Girinimbine	2	*Lys251, Glu248, Pro250, Lys245*	Conventional hydrogen bond, Pi-Alkyl, Alkyl	Hydrogen bond (Lys245= 2.13 and Glu248= 2.18) Pi Alkyl (Lys251= 4.51, Pro251= 4.43, Lys245= 5.31) Alkyl (Lys245= 4.18)
Andrographolide	4	*Pro250, Glu248, Lys245, Ile263, Gly217*	Conventional hydrogen bond, Alkyl	Conventional hydrogen bond (*Glu248= 4.89, Lys245= 4.96, Ile263 = 2.11, Gly217= 2.88*), Alkyl (Pro250= 4.00, 4.07, 5.05)
Berberine	2	*Ile334, Glu168, Val296, Val330, Thr333*	Conventional hydrogen bond, Carbon hydrogen bond, Pi-Alkyl, Alkyl, Pi-Sigma	Conventional hydrogen bond (*Ile334= 2.38, Glu168= 4.85*), Carbon hydrogen bond (Ile334=2.95), Pi-Alkyl (Val 296=4.15, 5.47), Alkyl (Val330= 4.36, 5.31), Pi-Sigma (Thr333 =3.62)
Sulforaphane	1	*Ala246, Asn265*	Conventional hydrogen bond, Carbon hydrogen bond	Conventional hydrogen bond (Ala 246= 4.94), Carbon hydrogen bond (*Asn265= 2.78)*
Resveratrol	3	*Lys245, Ile263, Asn265, Phe189, Arg311, Pro250, Lys160*	Conventional hydrogen bond, Pi-Pi T-shaped, Pi-alkyl, Pi-cation	Conventional hydrogen bond (*Lys245= 2.12, Ile263=2.14, Asn265= 2.26*), Pi-Pi T-shaped (*Phe189=4.98*), Pi-alkyl (*Pro250 = ,4.05, Lys160=5.45*), Pi-cation (*Arg311 = 3.62*)
Oridonin	2	*Lys245, Phe189, Pro250*	Conventional hydrogen bond, Pi-alkyl, Alkyl	Conventional hydrogen bond (*Lys245=1.69, 2.15)*, Pi-alkyl (*Phe189=4.64, 4.94)*, Alkyl (Pro250=4.20, 4.77, 3.77 Lys245= 2.01)
Obovatol	3	*ILE263, Asn265, Phe189, Phe188, Lys245, Pro250*	Conventional hydrogen bond, Pi-Pi T-shaped, Alkyl, Pi-alkyl	Conventional hydrogen bond (*ILE263= 2.03, Asn265=4.94, 4.96,*), Pi-Pi T-shaped (Phe189= 4.80), Alkyl (*Phe188 = 4.49, Lys245= 3.83*), Pi-alkyl (Pro250= 3.89)
Niclosamide	3	*Lys335, Lys162, Thr313, Arg311, Phe314*	Conventional hydrogen bond, Pi-cation, Pi-Sigma, Alkyl, Pi-Alkyl	Conventional hydrogen bond (*Lys335= 2.36 , Lys162=2.07, Thr313=2.08*), Pi-cation (Lys162= 3.24), Pi-Sigma (Thr313= 3.09), Alkyl (*Lys335= 5.49, Arg311= 4.29, 4.72)*, Pi-Alkyl (Phe314= 4.88
4-sulfonic calixarene	6	*Lys335,Lys162, Arg311, Lys160,Leu159, Ala161, Lys198, Lys163*	Conventional hydrogen bond, Carbon hydrogen bond, Pi-Cation	Conventional hydrogen bond (Lys335=2.42, Arg311=2.49, Lys160= 2.42, Leu159=2.10, Ala161=2.23, 2.04, Lys198=2.07), Carbon hydrogen bond (Lys163=3.67), Pi-Cation (Lys162=3.88)

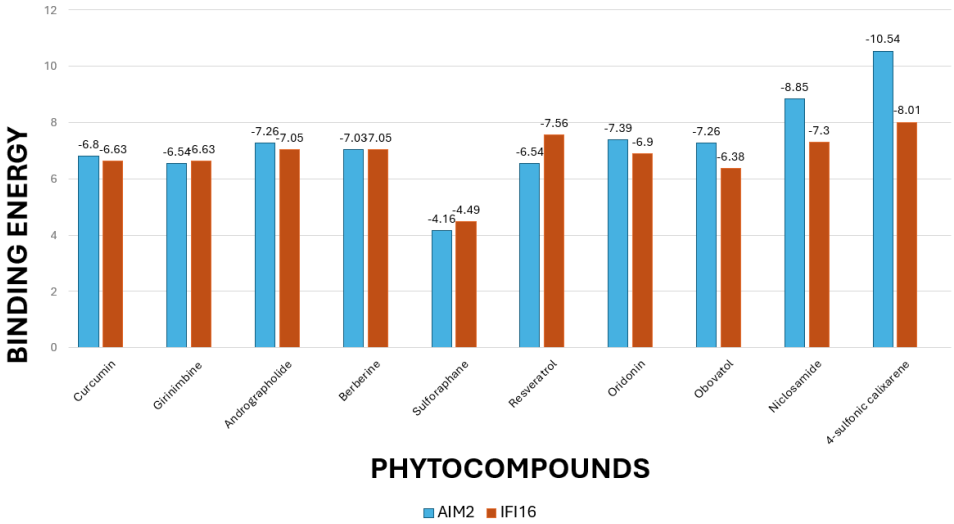

Figure 1. Binding affinity of AIM2 & IFI16 with selected phytocompounds

Similarly, the binding affinities of the ligands to IFI16 were: -6.63 kcal/mol (Curcumin), -6.63 kcal/mol (Girinimbine), -7.05 kcal/mol (Andrographolide), -7.07 kcal/mol (Berberine), -4.49 kcal/mol (Sulforaphane), -7.56 kcal/mol (Resveratrol), -6.90 kcal/mol (Oridonin), -6.38 kcal/mol (Obovatol), -7.30 kcal/mol (Niclosamide), and -8.01 kcal/mol (4-sulfonic calixarene) **(Figure 1)**. Here, 4-sulfonic calixarene exhibited the highest affinity toward IFI16, forming seven hydrogen bonds. Among the phytocompounds, Resveratrol displayed the strongest affinity, followed by Berberine, Andrographolide, Oridonin, Curcumin, and Girinimbine, with Sulforaphane showing the lowest affinity. Docking analysis also revealed that Resveratrol formed six hydrogen bonds with IFI16, while Andrographolide formed five. Curcumin and Obovatol each formed three hydrogen bonds **(Table 3)**.

Table 3. Docking analysis of IFI16 with selected phytocompounds

Ligand	No of hydrogen bonds	Interacting amino acid	Interacting bonds	Bond length
Curcumin	4	*Tyr317, Ile315, His241, Ala298, Arg297, Phe239, Asp268*	Conventional hydrogen bond, Carbon-hydrogen bond, Pi-Sigma, Pi-Pi-T shaped, Alkyl	hydrogen bond (Tyr317= 2.17, Phe239= 2.91, *Arg297*= 2.80, *Asp268* =2.24) Carbon-hydrogen bond (Ala298= 3.05) Pi-sigma (Tyr317= 4.39), Pi-Pi-T shaped (Ile315=4.93) Alkyl (Phe239=4.40)
Girinimbine	1	*Glu275, Leu245, Ile227, Lys226*	Conventional hydrogen bond, Pi-anion, Pi-Lone pair, Alkyl, Pi-alkyl	hydrogen bond (Glu275= 2.06), Pi-anion (Glu 275= 4.61, 4.56), Pi-Lone pair (Leu245 =2.78) Alkyl (Lys226 = 4.51, 4.84, 5.09, 5.02), Pi-alkyl (ile227= 4.33, 5.26, 5.21)
Andrographolide	5	*Glu300,Tyr317, Leu302, Gln310, Val316*	Conventional hydrogen bond, Alkyl	Conventional hydrogen bond (*Glu300= 2.04, 2.90,Tyr317= 2.27, Leu302= 2.20, Gln310= 2.03,*), Alkyl (*Val316 = 5.34, Leu302*)= 5.08
Berberine	2	*Gln238, Thr235, Phe240, Val205, Ile206, Phe288*	Conventional hydrogen bond, Pi-Sigma, Pi-Pi Stacked, Alkyl, Pi- Alkyl	Conventional hydrogen bond (*Gln238= 4.96, 2.55, Thr235=2.09)*, Pi-Sigma (*Thr235=3.52*), Pi-Pi Stacked (*, Phe288=4.73*), Alkyl (*Val205= 4.99, 4.61, Ile2064.93, 4.73*), Pi- Alkyl (*Phe88= 4.49,* Phe240= 4.93)
Sulforaphane	1	*Tyr317, His241, Phe239*	Conventional hydrogen bond, Pi donor hydrogen bond, Unfavourable positive positive	Conventional hydrogen bond (*Tyr317=1.99*), Pi donor hydrogen bond (*Phe239=4.17*), Unfavourable positive positive (*His241= 4.64*)

Resveratrol	6	*Ile315, Gln310, Tyr317, Leu302, Val316, His241, Ser269*	Conventional hydrogen bond, Pi-cation, Pi-Donor hydrogen bond, Pi-Sigma, Pi Pi T shaped, Pi-Alkyl	Conventional hydrogen bond (*Ile315 = 2.76, Gln310=2.78, Tyr317=2.06, Leu302=1.88, His241=4.98, Ser269=1.72*), Pi-cation (His241=4.02), Pi-Donor hydrogen bond (Tyr 317= 3.96), Pi-Sigma (Val316=3.82), Pi Pi T shaped (His241=4.16), Pi-Alkyl (Leu302=4.57)
Oridonin	2	*Arg297, Ile315, His241, Val316, Leu302, Phe239*	Conventional hydrogen bond, Pi-Sigma, Alkyl, Pi-Alkyl, Unfavorable Donor-Donor	Conventional hydrogen bond (*Arg297=2.94, Ile315=2.28*), Pi-Sigma (Phe239=3.66), Alkyl (His241=5.23, 4.78, Val316=4.91), Pi-Alkyl (Leu302=4.05), Unfavorable Donor-Donor (Arg297=2.08)
Obovatol	3	*His241, Asp268, Ser269, Tyr 317,Phe239, Phe240*	Conventional hydrogen bond, Carbon hydrogen bond, Pi-cation, Pi-sigma, Pi-lone pair, Pi-Pi-T shaped, Pi-alkyl	Conventional hydrogen bond (*His241=2.51, Asp268= 2.16, Ser269=2.32*), Carbon hydrogen bond (Phe240=3.65), Pi-cation (His241=4.26), Pi-sigma (Phe239=4.61), Pi-lone pair (Phe239=2.92), Pi-Pi-T shaped (Tyr317= 5.42), Pi-alkyl (His241=4.39, Tyr317= 4.70)
Niclosamide	6	*Gln363, Ser211, Lys289, Lys299, Thr301, Val319*	Conventional hydrogen bond Unfavorable Donor-Donor, Pi-cation, Alkyl, Pi-Alkyl	Conventional hydrogen bond (*Gln363=2.71, Ser211=1.96, Lys289=2.13, Lys299=2.18, 2.09, Thr301=1.96*), Unfavorable Donor-Donor (*Thr301=2.42)*, Pi-cation (Lys389=4.21), Alkyl (Val319=4.17,5.25, 4.79), Pi-Alkyl (Lys299=3.84)
4-sulfonic Calixarene	8	*Lys389, Lys299, Lys361, Thr301, Val319, Met321, Lys303*	Conventional hydrogen bond, Pi-Alkyl	Conventional hydrogen bond (*Lys389=2.19, Lys299=2.06, Lys361=2.03,2.31, Thr301=4.85, Val319=1,98, Met321=2.76, Lys303=2.04*), Pi-Alkyl (Val319=4.82)

Given their strong binding affinities and several hydrogen bonds with both AIM2 and IFI16, Resveratrol and Andrographolide were selected for further molecular dynamics simulations with these targets. The docked model of the four complexes is represented in **Figure 2**.

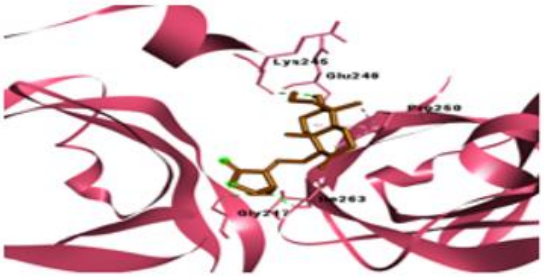

a) ANDROGRAPHOLIDE WITH AIM2

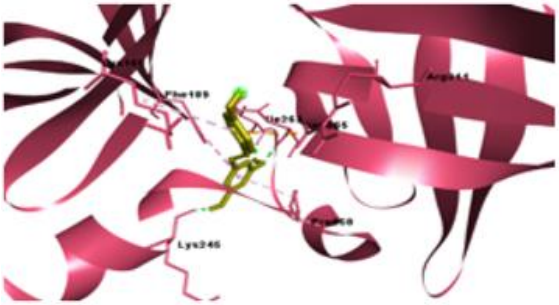

b) RESVERATROL WITH AIM2

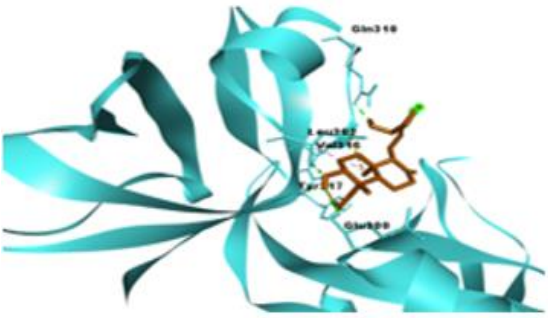

c) ANDROGRAPHOLIDE WITH IFI16

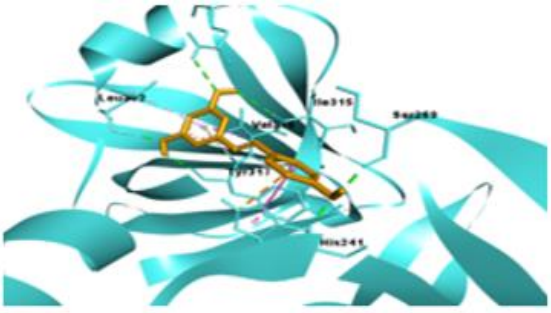

d) RESVERATROL WITH IFI16

Figure 2. Docked model of AIM2 & IFI16 with andrographolide and resveratrol

The molecular dynamics simulation of AIM2 with andrographolide and resveratrol revealed that the Root Mean

Square Deviation (RMSD) of 3RN2-APO, 3RN2-AND, and 3RN2-RES complexes remained stable up to 100 ns, suggesting the docked complexes were stable throughout the simulation. The average RMSD values were 0.30 ± 0.06 nm for 3RN2-APO, 0.31 ± 0.04 nm for 3RN2-AND, and 0.29 ± 0.01 nm for 3RN2-RES, indicating minimal fluctuations and a stable complex system in both 3RN2-AND and 3RN2-RES. Root Mean Square Fluctuation (RMSF) values were also calculated for each residue in the 3RN2-APO, 3RN2-AND, and 3RN2-RES complexes, with average values of 0.15 ± 0.08 nm, 0.17 ± 0.08 nm, and 0.17 ± 0.07 nm, respectively, showing no significant deviation in RMSF distribution among the complexes **(Figure 3)**.

The radius of gyration (Rg) values were 1.82 ± 0.03 nm, 1.81 ± 0.02 nm, and 1.79 ± 0.02 nm for 3RN2-APO, 3RN2-AND, and 3RN2-RES, respectively, indicating similar compactness across the systems. The solvent-accessible surface area (SASA) values showed consistent equilibration across the simulation, with averages of 118.08 ± 2.89 nm² for 3RN2-APO, 120.04 ± 2.38 nm² for 3RN2-AND, and 110.55 ± 4.76 nm² for 3RN2-RES **(Figure 3)**.

Intra-molecular hydrogen bond analysis showed averages of 134.90 ± 6.24 for 3RN2-APO, 135.45 ± 6.21 for 3RN2-AND, and 138.22 ± 7.55 for 3RN2-RES, with the complexes forming more hydrogen bonds in 3RN2-AND and 3RN2-RES than in 3RN2-APO, contributing to increased stability. The time-dependent analysis of hydrogen bonds confirmed that 3RN2-AND formed 1 to 5 hydrogen bonds, and 3RN2-RES formed 1 to 9 hydrogen bonds consistently throughout the simulation. Principal component analysis (PCA) indicated reduced flexibility across both eigenvectors (EVs), with the 3RN2-APO, 3RN2-AND, and 3RN2-RES complexes occupying overlapping conformational spaces. This limited movement indicates that 3RN2-AND and 3RN2-RES did not significantly alter the target structure's dynamics, supporting complex stability **(Figure 3)**.

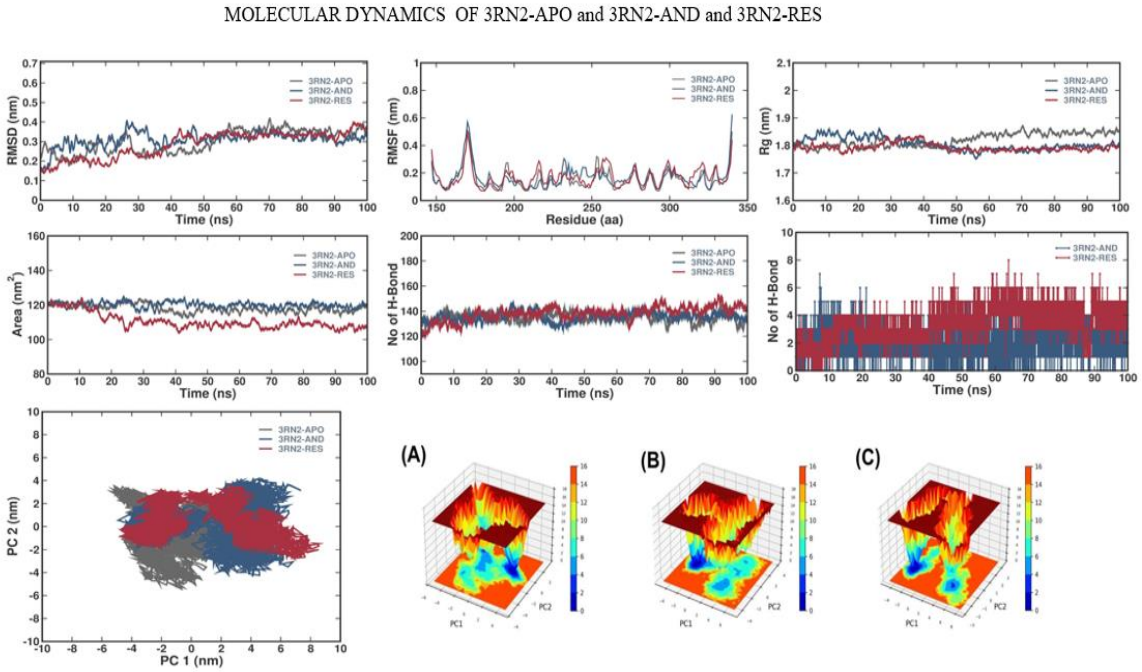

Figure 3. Molecular dynamics of 3RN2-AND and 3RN2-RES complexes

Free energy landscape (FEL) plots for principal components 1 and 2 (PC1 and PC2) showed deeper blue regions in both 3RN2-AND and 3RN2-RES, indicating a stable protein conformation with lower energy levels (ranging from 0 to 8 kJ/mol for 3RN2-APO, 0 to 7 kJ/mol for 3RN2-AND, and 0 to 9 kJ/mol for 3RN2-RES). Each complex displayed a single global minimum within a local basin, suggesting that 3RN2-AND and 3RN2-RES did not induce significant conformational changes, thus stabilizing the target structure **(Figure 3)**. Binding affinity was evaluated using the MM-PBSA method, yielding total binding energies of -112.100 ± 18.106 kJ/mol for 3RN2-AND and -15.328 ± 2.539 kJ/mol for 3RN2-RES.

Similarly, the molecular dynamics simulation of IFI16 with andrographolide and resveratrol showed the average RMSD for the 8X70-APO, 8X70-AND, and 8X70-RES complexes was 0.36 ± 0.06 nm, 0.27 ± 0.04 nm, and 0.28 ± 0.04 nm, respectively, indicating stability throughout the simulation. The RMSF values were also stable, with averages of 0.15 ± 0.08 nm, 0.14 ± 0.08 nm, and 0.12 ± 0.07 nm for 8X70-APO, 8X70-AND, and 8X70-RES, showing consistency across the complexes. Rg values indicated comparable compactness, with averages of 1.77 ± 0.01 nm, 1.76 ± 0.01 nm, and 1.74 ± 0.01 nm for 8X70-APO, 8X70-AND, and 8X70-RES. SASA values showed equilibration with averages of 109.76 ± 6.29 nm² for 8X70-APO, 116.87 ± 3.38 nm² for 8X70-AND, and 109.82 ± 3.67 nm² for 8X70-RES **(Figure 4)**.

Intra-hydrogen bonding analysis revealed higher bond stability in 8X70-AND and 8X70-RES compared to 8X70-APO, with average

values of 138.96 ± 8.15, 134.24 ± 5.95, and 138.35 ± 6.81 for 8X70-APO, 8X70-AND, and 8X70-RES, respectively. PCA analysis confirmed that 8X70-AND and 8X70-RES did not significantly alter the target's dynamics. FEL analysis for the 8X70 complexes displayed energy values ranging from 0 to 16 kJ/mol for 8X70-APO and 8X70-AND, and 0 to 14 kJ/mol for 8X70-RES, with a single global minimum, suggesting stability without significant conformational changes **(Figure 4)**.

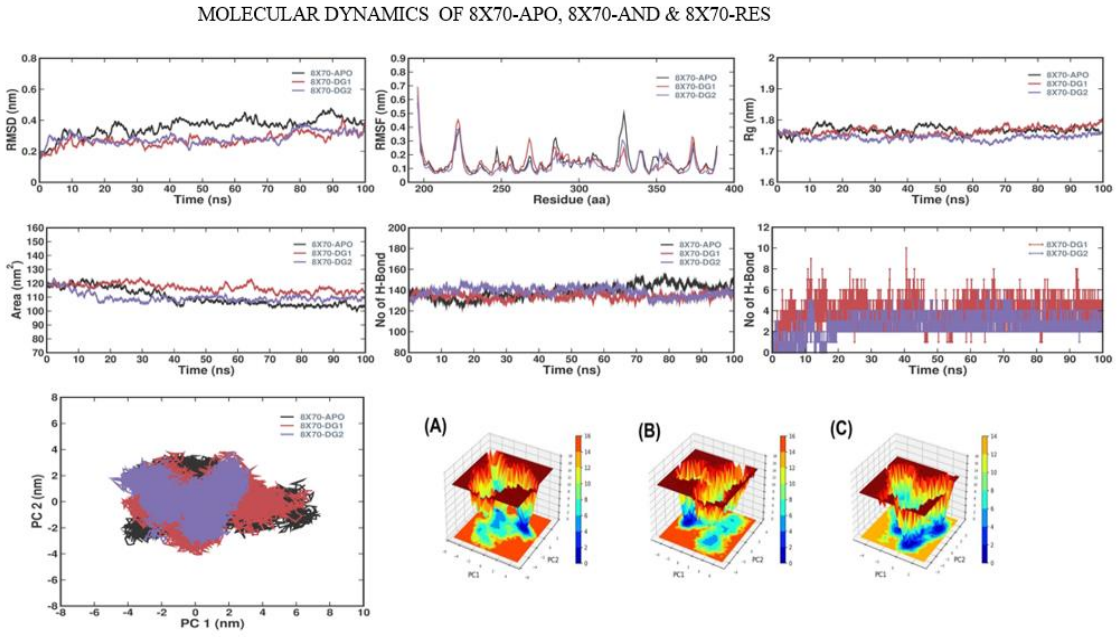

Figure 4. Molecular dynamics of 8X70-AND & 8X70-RES complexes

In the AIM2-andrographolide complex, glutamine, isoleucine, lysine, and glycine were the interacting amino acids, forming four hydrogen bonds. In contrast, the IFI16-andrographolide complex demonstrated interactions with glutamic acid, tyrosine, leucine, and glutamine, forming five hydrogen bonds. The binding energies of both complexes were greater than -7 kcal/mol, signifying a strong affinity for these complexes. The resveratrol-AIM2 complex presented a binding affinity of -6.54 kcal/mol, where lysine, leucine, and asparagine contributed three hydrogen bonds. The resveratrol-IFI16 complex formed six hydrogen bonds with isoleucine, lysine, leucine, histidine, glutamine, and serine, yielding a binding energy of -7.56 kcal/mol. Hydrogen bonds, as known facilitators of protein-ligand binding, play a key role in determining ligand specificity, complex stability, and influencing drug selectivity and affinity (Bissantz *et al*., 2010). Compared to the other phytocompounds, both andrographolide and resveratrol exhibited stable and strong affinities with AIM2 and IFI16, demonstrating their potential as viable therapeutic candidates for modulating inflammasome activity. However, the Poisson-Boltzmann surface area (MM-PBSA) method indicated that AIM2-andrographolide and IFI16-andrographolide exhibited higher binding affinity compared to AIM2-resveratrol and IFI16-resveratrol.

Resveratrol, isolated from grape skin, peanuts, and berries has anti-inflammatory and antioxidant properties (Zhang *et al*., 2021). It directly suppresses the release of proinflammatory cytokines in a wide range of tissues (Soufi *et al*., 2012; Natalin *et al*., 2016). Resveratrol supplementation has been shown to reduce inflammatory markers in patients with chronic periodontitis (Nikniaz *et al*., 2023). Andrographolide, extracted from Andrographis paniculata, has been widely used in Indian and Chinese medicine to treat infections. Other than antibacterial activity, it possesses anti-inflammatory, antiviral, and immunomodulatory properties (Kishore *et al*., 2017). It reduces the levels of proinflammatory cytokines, and reactive oxygen species levels in respiratory diseases (Peng *et al*., 2016). It is employed as a conservative agent in radiation-induced lung injury and inhibits the transport of AIM2 to the nucleus to detect DNA damage (Gao *et al*., 2019). A study by Ambili *et al*. (2017), has suggested andrographolide as a promising host-modulatory therapy due to its inhibition of NF-κβ activation and suppression of bone resorption genes in cultured fibroblasts. This study is the first to evaluate the docking and simulation of andrographolide with AIM2 and IFI16, demonstrating its potential in effectively inhibiting inflammasome activity and the results suggest that andrographolide may serve as a novel, adjunctive phytocompound-based host modulatory therapy in the management of periodontal disease.

Conclusion

This study highlights the promising therapeutic potential of phytocompounds andrographolide and resveratrol in modulating DNA-sensing inflammasome activity in periodontitis. Both compounds demonstrated high binding affinities with AIM2 and IFI16, forming stable protein-ligand complexes that were further

validated through molecular dynamics simulations. Andrographolide, in particular, exhibited superior binding energy and complex stability, suggesting a stronger inhibitory effect on inflammasome activation compared to resveratrol. Andrographolide could serve as a novel host modulatory agent targeting inflammasome-mediated periodontal destruction. Further, in vivo studies are warranted to validate their efficacy and safety in clinical settings.

Acknowledgments: The authors thank Dr. Ananthi Sivagnanam and Dr. Vivek Chandramohan for their assistance in carrying out the in silico analysis.

Conflict of interest: None

Financial support: None

Ethics statement: None

References

Almine, J. F., O'Hare, C. A., Dunphy, G., Haga, I. R., Naik, R. J., Atrih, A., Connolly, D. J., Taylor, J., Kelsall, I. R., Bowie, A. G., et al. (2017). IFI16 and cGAS cooperate in the activation of STING during DNA sensing in human keratinocytes. *Nature Communications*, *8*(1), 14392.

Ambili, R., Janam, P., Babu, P. S., Prasad, M., Vinod, D., Kumar, P. A., Kumary, T. V., Nair, S. A., & Pillai, M. R. (2017). An ex vivo evaluation of the efficacy of andrographolide in modulating differential expression of transcription factors and target genes in periodontal cells and its potential role in treating periodontal diseases. *Journal of Ethnopharmacology*, *196*, 160-167.

Bissantz, C., Kuhn, B., & Stahl, M. (2010). A medicinal chemist's guide to molecular interactions. *Journal of Medicinal Chemistry*, *53*(14), 5061-5084.

Cekici, A., Kantarci, A., Hasturk, H., & Van Dyke, T. E. (2014). Inflammatory and immune pathways in the pathogenesis of periodontal disease. *Periodontology 2000*, *64*(1), 57-80.

Daina, A., Michielin, O., & Zoete, V. (2017). SwissADME: A free web tool to evaluate pharmacokinetics, drug-likeness and medicinal chemistry friendliness of small molecules. *Scientific Reports*, *7*(1), 42717.

Gangadharappa, B. S., Sharath, R., Revanasiddappa, P. D., Chandramohan, V., Balasubramaniam, M., & Vardhineni, T. P. (2020). Structural insights of metallo-beta-lactamase revealed an effective way of inhibition of enzyme by natural inhibitors. *Journal of Biomolecular Structure and Dynamics*, *38*(13), 3757-3771.

Gao, J., Peng, S., Shan, X., Deng, G., Shen, L., Sun, J., Jiang, C., Yang, X., Chang, Z., Sun, X., et al. (2019). Inhibition of AIM2 inflammasome-mediated pyroptosis by Andrographolide contributes to amelioration of radiation-induced lung inflammation and fibrosis. *Cell Death & Disease*, *10*(12), 957.

Kishore, V., Sastry Yarla, N., Bishayee, A., Putta, S., Malla, R., Rao Reddy Neelapu, N., Challa, S., Das, S., Shiralgi, Y., Hegde, G., et al. (2017). Multi-targeting andrographolide and its natural analogs as potential therapeutic agents. *Current Topics in Medicinal Chemistry*, *17*(8), 845-857.

Kumari, R., Kumar, R., Open Source Drug Discovery Consortium, & Lynn, A. (2014). g_mmpbsa--a GROMACS tool for high-throughput MM-PBSA calculations. *Journal of Chemical Information and Modeling*, *54*(7), 1951-1962.

Lamkanfi, M., & Dixit, V. M. (2014). Mechanisms and functions of inflammasomes. *Cell*, *157*(5), 1013-1022.

Man, S. M., Karki, R., & Kanneganti, T. D. (2016). AIM2 inflammasome in infection, cancer, and autoimmunity: Role in DNA sensing, inflammation, and innate immunity. *European Journal of Immunology*, *46*(2), 269-280.

Marchesan, J. T. (2020). Inflammasomes as contributors to periodontal disease. *Journal of Periodontology*, *91*, S6-S11.

Morris, G. M., Huey, R., Lindstrom, W., Sanner, M. F., Belew, R. K., Goodsell, D. S., & Olson, A. J. (2009). AutoDock4 and AutoDockTools4: Automated docking with selective receptor flexibility. *Journal of Computational Chemistry*, *30*(16), 2785-2791.

Natalin, H. M., Garcia, A. F. E., Ramalho, L. N. Z., & Restini, C. B. A. (2016). Resveratrol improves vasoprotective effects of captopril on aortic remodeling and fibrosis triggered by renovascular hypertension. *Cardiovascular Pathology*, *25*(2), 116-119.

Nikniaz, S., Vaziri, F., & Mansouri, R. (2023). Impact of resveratrol supplementation on clinical parameters and inflammatory markers in patients with chronic periodontitis: A randomized clinical trail. *BMC Oral Health*, *23*(1), 177.

Olcum, M., Tastan, B., Ercan, I., Eltutan, I. B., & Genc, S. (2020). Inhibitory effects of phytochemicals on NLRP3 inflammasome activation: A review. *Phytomedicine*, *75*, 153238.

Özenver, N., & Efferth, T. (2021). Phytochemical inhibitors of the NLRP3 inflammasome for the treatment of inflammatory diseases. *Pharmacological Research*, *170*, 105710.

Papathanasiou, E., Alreshaid, R., & Araujo de Godoi, M. (2023). Anti-inflammatory benefits of food ingredients in periodontal diseases. *Pathogens*, *12*(4), 520.

Peng, S., Gao, J., Liu, W., Jiang, C., Yang, X., Sun, Y., Guo, W., & Xu, Q. (2016). Andrographolide ameliorates OVA-induced lung injury in mice by suppressing ROS-mediated NF-κB signaling and NLRP3 inflammasome activation. *Oncotarget*, *7*(49), 80262.

Soufi, F. G., Mohammad-Nejad, D., & Ahmadieh, H. (2012). Resveratrol improves diabetic retinopathy possibly through oxidative stress—Nuclear factor κB—Apoptosis pathway. *Pharmacological Reports*, *64*(6), 1505-1514.

Zhang, L. X., Li, C. X., Kakar, M. U., Khan, M. S., Wu, P. F., Amir, R. M., Dai, D. F., Naveed, M., Li, Q. Y., Saeed, M., et al. (2021). Resveratrol (RV): A pharmacological review and call for further research. *Biomedicine & Pharmacotherapy*, *143*, 112164.